Optics Letters

Compact interferometric module for full-field interferometric phase microscopy with low spatial coherence illumination

Amit Nativ and Natan T. Shaked*

Department of Biomedical Engineering, Tel Aviv University, Tel Aviv, Israel
*Corresponding author: nshaked@tau.ac.il

We propose a compact and external off-axis interferometric module that can achieve interference with low spatial coherence illumination over the entire field of view. The interferometer is easy to align and stable and can be connected to the output of an existing microscope illuminated with a low spatial coherence light source, thus allowing quantitative phase imaging with a low degree of spatial noise. We demonstrate the imaging and the interference properties of the proposed interferometric module and use it for quantitative phase imaging of reflective samples.　　© 2017 Optical Society of America

Interferometric phase microscopy (IPM), also called digital holographic microscopy, uses interference to record the complex wavefront of light interacting with the sample. By digital post-processing of the interference pattern, it is possible to quantitatively reconstruct both the amplitude and the phase of the sample. IPM measures the quantitative phase profile, which is proportional to the optical path delay (OPD) profile of the sample, hence allowing imaging of transparent objects or profiling reflective surfaces.

In common-path interferometry, the sample and the reference beams propagate together in most of their optical paths, yielding decreased differential noise between the beams and increased temporal stability [1]. In off-axis interferometry, there is a small angle between the sample and the reference beams, which enables obtaining the quantitative phase map in a single camera exposure, allowing acquisition of highly dynamic samples [2].

We have lately proposed the off-axis τ interferometer [3], a compact external interferometric module that can be connected to an existing microscope, and allows obtaining the quantitative phase profile in a single camera exposure. This is done by splitting the image in the output of the microscope using optical spatial

filtering to erase the sample spatial modulation from one of the beams, and combining the beams on the camera at a small angle created by a retro-reflector, generating off-axis interference fringes that capture the sample quantitative phase profile.

Using highly coherent illumination in interferometric imaging makes it easy to obtain high-visibility off-axis interference fringes on the entire sensor. However, imaging with a highly coherent light source degrades the output image quality due to parasitic interferences, speckle noise, and ringing artifacts around sharp edges [4–7], thus, damaging the ability to measure small spatial changes. This limitation can be solved by using low-temporal-coherence illumination and matching the total optical paths of the beams to allow the creation of interference. However, off-axis interference with low-temporal-coherence sources is hard to obtain since, across the off-axis interferogram created on the camera, the optical path difference between the sample and the reference beams might be longer than the coherence length of the source, precluding the generation of high-visibly interference [8,9]. The practical meaning of this limitation is that the sample cannot be simultaneously recorded by off-axis interferometry on the entire camera sensor using low-coherence sources [10]. By tilting the wave field of one of the beams to coincide with the non-tilted beam, off-axis interference can be obtained on the entire camera sensor. This can be achieved by utilizing diffraction gratings [11,12] or specialized prisms [13,14]. This solution, however, induces an increased size of the interferometer. For example, if a diffraction grating is used [11], the off-axis angle between the beams is created by an angular shift between the 0 and +1 orders of the grating, and the two beams still need to be projected on the camera at a suitable off-axis angle, after spatially filtering one of the beams. This results in a long 4f lens configuration between the grating and the camera.

Unfortunately, although our previous off-axis τ interferometric module is compact, it cannot work with low-temporal-coherence illumination and still obtain equal-visibility off-axis interference fringes on the entire camera sensor, basically because it uses a refractive beam splitter to split the beams. In addition, this previous design cannot work with a low-spatial-coherence source, due to the fact that a retro-reflector is positioned only in the sample beam path, inducing flipping

of the field only in one of the beams and, thus, nonmatching spatial coherence areas. Another drawback is that the reference beam of the off-axis τ interferometric module passes twice through the pinhole, causing a power loss.

Another approach to reduce coherent noise is to decrease the spatial coherence of the illumination. This can be done in a controlled manner by transmitting a laser through a rotating ground glass [15,16].

In this Letter, we suggest a new compact interferometer, termed as the partial-coherence off-axis τ interferometer (PC τ), which does not require a grating, but can still work under low spatial coherence illumination. Figure 1(a) presents a low spatial coherence light source, built out of a DPSS laser (532 nm, 96.1 mW, Laser Glow Technologies) followed by a rotating diffuser (Thorlabs N-BK7 ground glass, 1500 grit, mounted on 2342S 012CR FAULHABER DC engine) and a spatial filter that controls the degree of spatial coherence of the source [lenses L_1 ($f_1 = 25.4$ mm), L_2 ($f_2 = 50$ mm), pinhole P_1, and L_3 ($f_3 = 100$ mm)]. The low spatial coherence source illuminates

Fig. 1. (a) Experimental system: a reflection microscope, illuminated by a low spatial coherence source, where the PC τ interferometric module is connected to its output. DPSS, diode pump solid state laser; D, diffuser; L_1–L_7, lenses; P_1, P_2, pinholes; BS_1, BS_2, cube beam splitters; MO, microscope objective; RR_1, RR_2, three-mirror retro-reflectors; S, sample beam; R, reference beam. (b) Three-mirror RR beam arrangement, ensuring that the beam reflected after hitting the RR three faces is at the same solid angle Ω as the incident beam, but flipped on both axes. (c) Photograph of the PC τ module (top view).

a reflection-mode microscope through lens L_4 ($f_4 = 250$ mm), and the light is directed to the sample through beam splitter BS_1 and microscope objective MO (Olympus MPLAPON50×, NA 0.95). The light reflected from the sample is magnified by the objective lens and is projected onto the output of the microscope by tube lens TL ($f_{TL} = 180$ mm). At the exit of the microscope, another 4f lens configuration is positioned for generating additional magnification [lens L_5 ($f_5 = 75$ mm) and lens L_6 ($f_6 = 100$ mm)], projecting the output image onto the input plane of the proposed compact interferometric module. In this module, beam splitter BS_2 splits the beam into two beams, whereas one of the beams turns into a reference beam using a spatial filter [lenses L_7 ($f_7 = 100$ mm), pinhole P_2, and L_8 ($f_8 = 180$ mm)]. This beam passes through the pinhole only once, increasing the power in the reference beam in comparison to our previous design. PLR_1 and PLR_2 are two polarizers used to equalize the intensity of the reference and the sample beams.

Significantly, in contrast to our previous design, PC τ uses a retro-reflector in each of the sample and the reference beam paths. However, simple two-mirror retro-reflectors are not enough to create an accurate spatial overlap of the sample and the reference beams on the camera, which is required for generating interference due to the low spatial coherence illumination. This is because any relative tilt between these retro-reflectors will decrease the overlapping area of the beams on the camera. Therefore, we suggest using a pair of three-mirror retro-reflectors (Spectrum Scientific, HCR-245-5AL). Note that we do not use prism retro-reflectors. As shown in Fig. 1(b), in a three-mirror retro-reflector, as long as the incident beam hits all three mirror faces, the solid angle of incidence and the solid angle of reflection are the same. Therefore, there is no tilt between the reference and the sample beams. This is true, even if a relative tilt between the two retro-reflectors exists due to mechanical misalignment. Hence, we achieve accurate spatial overlap between the beams over the full field of view (FOV), yielding high-visibility off-axis interference on the entire sensor.

After acquiring the off-axis interference by a single camera exposure, it is processed to the OPD map of the sample by using digital spatial filtering of one of the cross-correlation orders [17], subtracting the phase of a sample-free interferogram to compensate for aberrations and beam curvatures, followed by digital phase unwrapping to solve 2π ambiguities, where the sample is optically thicker than the wavelength [18].

To compare the new setup with our previous design, we first experimentally implemented both of them while illuminated with a low spatial coherence source. For this comparison, we used the rotating diffuser in front of the DPSS laser and set the diameter of pinhole P_1 to be 400 μm. We then measured the power spectrum of the resulting illumination beam and used it to calculate the spatial coherence function [5]. We obtained coherence radius ρ_c of 3 μm and an effective condenser numerical aperture NA_{cond} of 0.19. Under these illumination conditions, we compared the previous and the proposed designs. To demonstrate the difference in the imaging properties of the two systems, we purposely did not use pinhole P2, so that we did not create a reference beam, and obtained two copies of the imaged object on the camera. Figure 2 shows the acquired interference for a silicon wafer reflective test target created by electron-beam etching. As shown in Fig. 2(a), in the old setup, since only one retro-reflector is used, the beams are flipped. Hence, only a small part of the FOV, which is inside
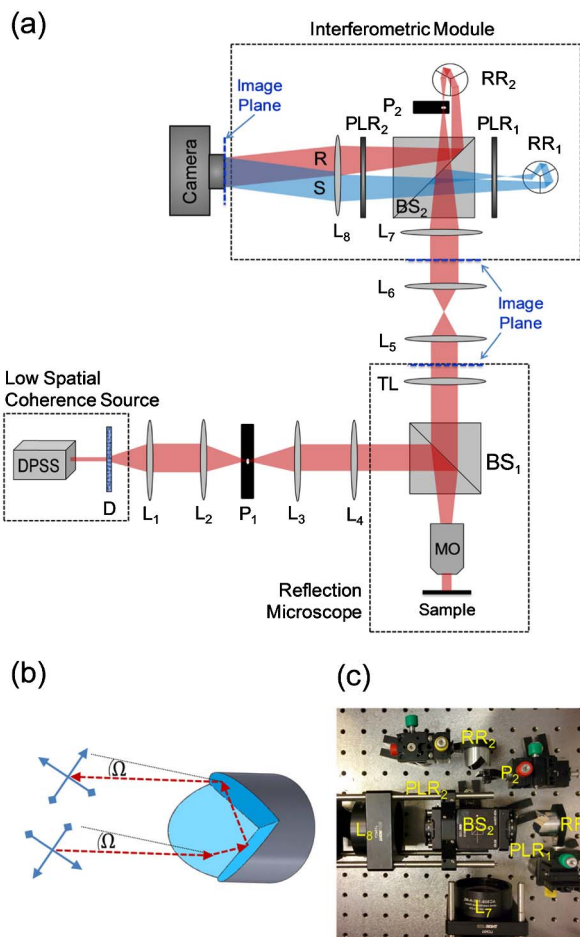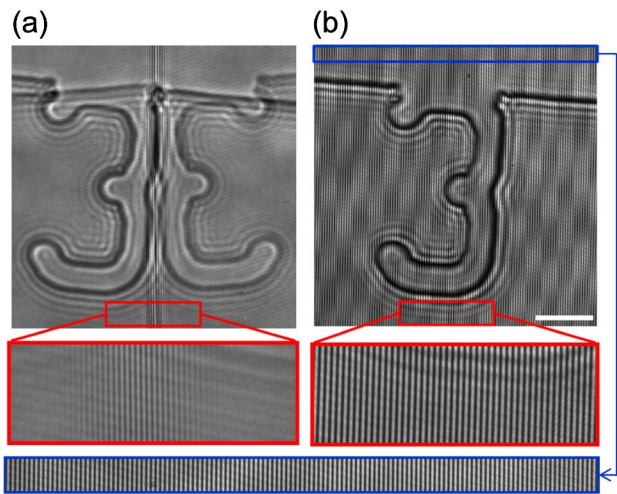
Fig. 2. Comparison of the imaging properties and the interference visibility between (a) the previous design and (b) the proposed design, both under low spatial coherence illumination and without using pinhole P2 (interfering two copies of the image). In (a), one of the images is flipped, and the interference area is limited. The spatial coherence radius used is $\rho_c = 3$ μm, which corresponds to the area of interference fringes in (a). In (b), on the other hand, both images fully overlap and high-visibility interference fringes are obtained on the entire camera FOV. The white scale bar represents 5 μm on the sample. See Visualization 1 for the interference obtained when shifting one of the RRs, demonstrating that this arrangement can obtain any spatial frequency of the off-axis interference on the entire camera FOV. To allow better visualization, the video was purposely recorded out of the image plane.

the coherence radius, has interference fringes, whereas the visibility of the interference decays rapidly outside the coherence radius. This means that it is not possible to acquire the interferogram of the sample on the entire camera FOV in case of using the previous design due to the low spatial coherence illumination used. In contrast, as shown in Fig. 2(b), in our new design, due to the use of a pair of three-mirror retro-reflectors, both images are perfectly aligned, with no relative spatial shift or tilt between the images. Most importantly, the interference fringes are strong and cover the entire FOV although low spatial coherence illumination is used.

Visualization 1 shows that the interference fringes can change their spatial frequency when shifting one of the RR in relation to the other one. In this case, the orientation of the two beams is always fixed due to the use of a pair of three-mirror retro-reflectors that keep the same solid angle between the beams. Thus, it is easy make the beams overlap so that high-visibility interference will be obtained on the entire camera FOV.

This feature of the proposed design ensures high-visibility interference, even when placing back pinhole P2 that creates a clear reference beam by spatial filtering. To demonstrate this, we used the previous and the proposed modules to measure the phase profile of an electron-beam etched silicon wafer with 60 nm high text on it. This height was verified by atomic force microscopy. We tried three degrees of spatial coherence: [P1 = 15 μm, NA$_{cond}$ = 0.09, $\rho_c = 28$ μm], [P1 = 100 μm, NA$_{cond}$ = 0.09, $\rho_c = 7$ μm], and [P1 = 200 μm, $\rho_c = 4$ μm, NA$_{cond}$ = 0.16]. Figure 3 shows the degradation in the OPD map quality due to the coherent noise created when increasing the spatial coherence of the illumination. Indeed, as shown in Fig. 4, the histograms of the OPD values in the background of
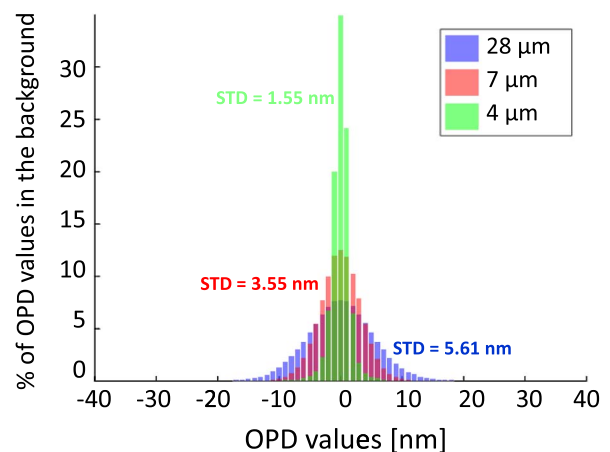

Fig. 4. Histograms of the OPD values in the background of the three OPD maps of different degrees of spatial coherences shown in Fig. 3, demonstrating the decrease in spatial noise obtained for lower degrees of spatial coherence. STD, standard deviation.
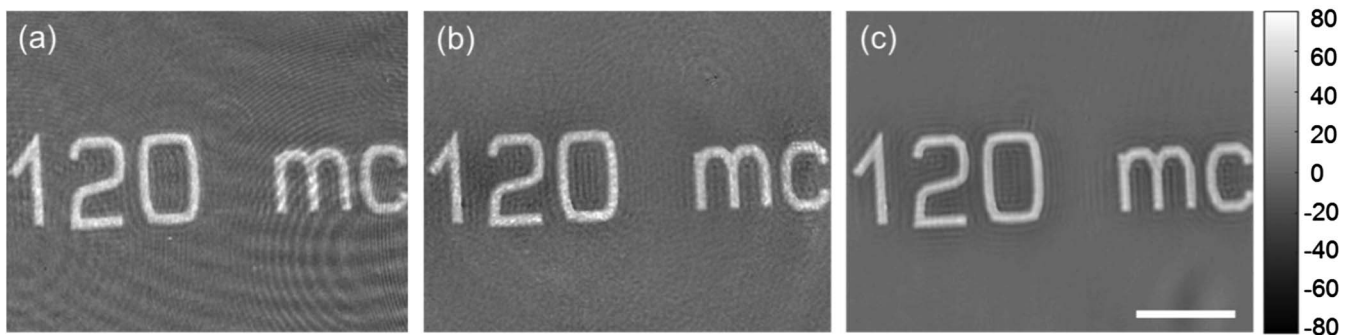

Fig. 3. OPD measurements with three degrees of spatial coherence of letters etched by an electron beam on a silicon wafer, demonstrating the decrease of spatial noise obtained when the spatial coherence of the illumination decreases. (a) High degree of spatial coherence; $\rho_c = 28$ μm, taken using the previous module. (b) Medium degree of spatial coherence; $\rho_c = 7$ μm, taken using the proposed PC τ module. (c) Low degree of spatial coherence; $\rho_c = 4$ μm, taken using the proposed PC τ module. The white scale bar represents 10 μm on the sample.

Figs. 3(a)–3(c) demonstrate that the spatial noise decrease coincides with the spatial coherence decrease.

In conclusion, we presented a compact and external interferometric module that is able to achieve a high fringe contrast on the entire camera FOV for low spatial coherence illumination. This interferometer, termed as PC τ, uses a pair of three-mirror retro-reflectors that preserves the solid angle of the incident and the reflected beams, hence keeping the reference and the sample beams always spatially aligned in relation to each other. We demonstrated the advantages of the unique imaging and the interference properties of the presented interferometric module in comparison with our previous design, which was limited in the interference area when using low-coherence illumination. We expect that the PC τ external module, being able to connect to existing imaging systems, will enhance IPM by providing low-noise profiling and quantitative phase maps for various clinical and industrial uses.

REFERENCES

1. V. Mico, Z. Zalevsky, and J. García, Opt. Commun. **281**, 4273 (2008).
2. S. Witte, A. Plauşka, M. C. Ridder, L. van Berge, H. D. Mansvelder, and M. L. Groot, Biomed. Opt. Express **3**, 2184 (2012).
3. P. Girshovitz and N. T. Shaked, Opt. Express **21**, 5701 (2013).
4. H. H. Hopkins, J. Opt. Soc. Am. **47**, 508 (1957).
5. C. Edwards, B. Bhaduri, T. Nguyen, B. G. Griffin, H. Pham, T. Kim, G. Popescu, and L. L. Goddard, Opt. Express **22**, 5133 (2014).
6. P. S. Considine, J. Opt. Soc. Am. **56**, 1001 (1966).
7. M. Wernick and G. Morris, Appl. Opt. **33**, 5906 (1994).
8. L. Martínez-León, G. Pedrini, and W. Osten, Appl. Opt. **44**, 3977 (2005).
9. F. Dubois, M. L. N. Requena, C. Minetti, O. Monnom, and E. Istasse, Appl. Opt. **43**, 1131 (2004).
10. M. Rinehart, Y. Zhu, and A. Wax, Biomed. Opt. Express **3**, 958 (2012).
11. B. Bhaduri, H. Pham, M. Mir, and G. Popescu, Opt. Lett. **37**, 1094 (2012).
12. M. Lošťák, R. Chmelík, M. Slabá, and T. Slabý, Opt. Express **22**, 4180 (2014).
13. Z. Monemhaghdoust, F. Montfort, Y. Emery, C. Depeursinge, and C. Moser, Biomed. Opt. Express **5**, 1721 (2014).
14. Z. Monemhaghdoust, F. Montfort, Y. Emery, C. Depeursinge, and C. Moser, Opt. Express **19**, 24005 (2011).
15. Y. Choi, T. D. Yang, K. J. Lee, and W. Choi, Opt. Lett. **36**, 2465 (2011).
16. R. Zhou, C. Edwards, A. Arbabi, G. Popescu, and L. L. Goddard, Nano Lett. **13**, 3716 (2013).
17. P. Girshovitz and N. T. Shaked, Opt. Lett. **39**, 2262 (2014).
18. O. Backoach, S. Kariv, P. Girshovitz, and N. T. Shaked, Opt. Express **24**, 3177 (2016).